PAPER

Tunable Tamm states at the interface of a 1D graphene-based photonic crystal and a nonlinear dielectric slab

IOP Publishing Physica Scripta
Phys. Scr. 95 (2020) 045504 (8pp) https://doi.org/10.1088/1402-4896/ab6799

Tunable Tamm states at the interface of a 1D graphene-based photonic crystal and a nonlinear dielectric slab

Samad Roshan Entezar and Babak Tavakkoly Moghaddam

Faculty of Physics, University of Tabriz, Tabriz, Iran

E-mail: s-roshan@tabrizu.ac.ir

Received 4 November 2019, revised 16 December 2019
Accepted for publication 3 January 2020
Published 18 February 2020

Abstract

We investigate the dispersion of the Tamm states at the interface of a 1D graphene-based photonic crystal and a nonlinear dielectric slab. We use the nonlinear transfer matrix method to obtain the dispersion of the Tamm states in both the graphene induced and Bragg gaps in the terahertz region. We explore the spectral tunability of the surface modes by adjusting parameters such as the thickness of the nonlinear slab, the intensity of the surface modes, and the chemical potential of graphene layers. We reveal that the penetration depth of the graphene induced bandgap modes in the uniform environment is several times greater than that of the conventional Bragg gap modes. Also, it is shown that we can improve the penetration depth of the surface modes by adjusting the thickness of the nonlinear slab, the intensity of the Tamm states, or the chemical potential of the graphene layers.

Keywords: Kerr-type nonlinearity, Tamm states, graphene, photonic crystal, chemical potential, penetration depth

(Some figures may appear in colour only in the online journal)

1. Introduction

In the last two decades, the surface electromagnetic waves (SEWs) have attracted the widespread attention of researchers. SEWs, which is utilized to study the physical features of the surfaces, have the potential to use in many applications and devices such as sensors, filters, microscopy, optical modulators, and in the enhancement of the nonlinear optical effects [1–5]. These non-radiative electromagnetic modes, which are evanescent perpendicular to the interface and propagate parallel to the interface between two media, sometimes called Bloch surface waves [6]. The SEWs which are supported by semi-infinite one-dimensional photonic crystals (1D-PCs) are called TAMM states [7–10]. Such a 1D-PC can be constructed from different materials including, dielectrics, semiconductors, metals, and graphene as the corresponding constituent elements of the structure. These materials play an essential role in the photonic bandgap (PBG) engineering [11–14].

Graphene, a flat monolayer of carbon atoms arranged in a honeycomb lattice, has gained much attention in recent years due to its unique thermal, mechanical, electrical, gate-controllable Fermi level, and optical/terahertz (THz) properties such as broadband optical absorption, ultrafast optical response and universal optical conductivity from visible to infrared [15–21]. Graphene has dissipative losses less than the usual metals at the THz and far-IR frequencies. Notably, the optical and electrical characteristics of the graphene are described by its frequency-dependent surface conductivity. It is found that the existence of SEWs depends on the conductivity of the graphene, which contains two interband and intraband contributions [22–25]. The optical conductivity of the graphene may be controlled and tuned using an external electric field which varies the chemical potential of graphene [15, 26]. Due to the experimental realization of the graphene monolayer and the layered structure composed of alternating graphene and dielectric layers [27, 28], there is an increasing interest to explore all optical properties of the graphene-based photonic crystal (GBPC). From this perspective, extensive

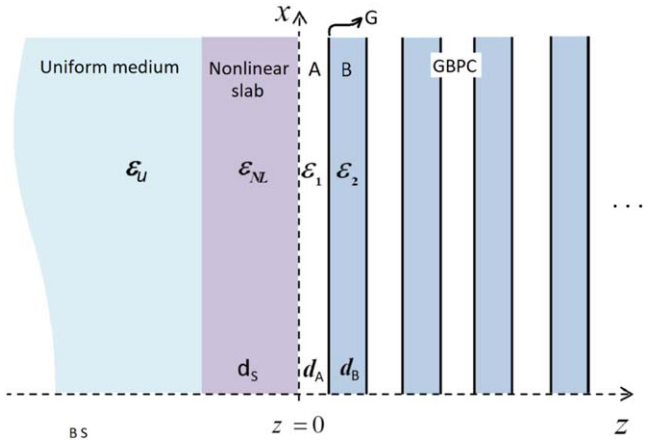

Figure 1. Geometry of the problem consist of a 1D GBPC and a nonlinear Kerr-type dielectric slab. Here, we assume that $d_A = 10\ \mu$m, $d_B = 10\ \mu$m, $d_S = 3d_A$, $\varepsilon_A = 4.84$, $\varepsilon_B = 2.29$, $\varepsilon_u = 1$.

studies have also been carried out in the realm of linear optical properties of the GBPCs. Among them, some researchers have examined linear Tamm states in the GBPCs to achieve the best local and tunable SEWs [29–33]. Contrary to the linear regime, the nonlinear optical properties of the GBPCs, especially nonlinear SEWs, have received less attention [34–38].

In this work, we theoretically investigate the dispersion properties of the TE-polarized Tamm states guided by the interface of a 1D GBPC and a nonlinear Kerr-type dielectric slab in THz region. We use the well-known transfer matrix method to calculate the PBGs of the 1D-PC and the dispersion of the nonlinear Tamm states. Then we discuss the intensity-dependent dispersion curves inside the first two bandgaps of the structure and explore the controllability of the dispersion of the Tamm states by adjusting parameters such as the thickness of the nonlinear slab, the intensity of the surface modes, and the chemical potential of graphene layers. The paper is organized as follows. In section 2, we introduce the model of the considered structure. The general calculated results and their analysis are presented in section 3. Finally, section 4 concludes with brief comments on the significance of the findings.

2. Theoretical model and calculations

Consider a semi-infinite 1D GBPC consists of alternative isotropic nonmagnetic dielectric layers A, B with the thicknesses d_A, d_B and the relative permittivities ε_A, and ε_B respectively, with the graphene monolayers G between them (see figure 1). A nonlinear Kerr-type dielectric slab of the thickness d_S and relative permittivity $\varepsilon_{\rm NL}$ from the left is attached to the GBPC. The relative permittivity of the Kerr-type nonlinear slab is given by [39, 40]:

$$\varepsilon_{\rm NL} = \varepsilon_S + \alpha|E|^2 \tag{1}$$

Here, ε_S is the linear part of the relative dielectric permittivity of the slab. The positive parameter α describes the Kerr-type nonlinearity. Also, the optical properties of the graphene monolayer, which is affected by the low absorption at the THz and far-IR frequencies, are given by the following dielectric function [41, 42]:

$$\varepsilon_g = 1 + \frac{{\rm i}\sigma_g(\omega)\eta_0}{k_0 d_g}, \tag{2}$$

where $\sigma_g(\omega)$ is the surface conductivity of the graphene monolayer given by the Kubo formula $\sigma_g(\omega) = \sigma_g^{\rm intra}(\omega) + \sigma_g^{\rm inter}(\omega)$ [23, 43]. Here

$$\sigma_g^{\rm intra}(\omega) = \frac{e^2}{4\hbar}\frac{\rm i}{2\pi}\left\{\frac{16\,k_{\rm B}T}{\hbar\omega}\ln\left(2\cosh\left(\frac{\mu_c}{2k_{\rm B}T}\right)\right)\right\},$$
$$\sigma_g^{\rm inter}(\omega) = \frac{e^2}{4\hbar}\{\frac{1}{2} + \frac{1}{\pi}\arctan\left(\frac{\hbar\omega - 2\mu_c}{2k_{\rm B}T}\right)$$
$$- \frac{\rm i}{2\pi}\ln\left(\frac{(\hbar\omega + 2\mu_c)^2}{(\hbar\omega - 2\mu_c)^2 + (2k_{\rm B}T)^2}\right)\}, \tag{3}$$

$k_0 = \omega/c$ is the vacuum wave number, $d_g = 0.334$ nm is the thickness of the graphene monolayer, η_0 is the impedance of the vacuum, T is the temperature, e is the charge of the electron, $k_{\rm B}$ is the Boltzmann constant, and μ_C is the chemical potential of the graphene monolayer which is determined by the electron density and can be varied with a gate voltage.

Consider a TE-polarized electromagnetic plane wave incident to the structure with its electric field in the y-direction of the used coordinates system in which the graphene monolayers are parallel to the x–y plane. Assume that $E_y = E(z){\rm e}^{{\rm i}k_0\beta x - {\rm i}\omega t}$ + c.c., which β is the component of the normalized wave number along the interface. We can determine the value of β during the excitation of the SEWs. One can generally excite the SEWs using prisms or gratings. If we use a prism, $\beta = n_p \sin(\theta_p)$ where n_p is the refractive index of the prism and θ_p is the incident angle of the beam used for excitation of the SEWs. The electric field amplitude $E(z)$ in the uniform medium on the left side of the nonlinear slab is given as $E(z) = E_0{\rm e}^{k_u(z+d_S)}$ for $z < -d_S$, which $k_u = k_0\sqrt{\beta^2 - \varepsilon_u}$ and E_0 is the electric field amplitude at $z = -d_S$. The value of E_0 depends on the intensity of the excitation beam. In the right-side with $z > 0$, the wave is the Bloch mode with

$$E(z) = \psi(z){\rm e}^{{\rm i}K_{\rm B}z}, \tag{4}$$

where $K_{\rm B}$ is the Bloch wave number, and $\psi(z)$ is the Bloch function which is a periodic function of z. At frequencies where the Bloch wave number has a complex value, the Bloch modes are evanescent. This condition defines the so-called forbidden bands of the periodic medium [44]. We use the transfer matrix method to investigate the forbidden bandgaps of the considered GBPC. One can easily show that the transfer matrix $M = M_A \times M_g \times M_B \times M_g$ relates the fields of two identical layers in the adjacent unit cells of the GBPC. Here M_A, M_B and M_g are defined as follows:

$$M_A = \begin{bmatrix} \cos k_{zA}d_A & \frac{\rm i}{\zeta_A}\sin k_{zA}d_A \\ {\rm i}\zeta_A \sin k_{zA}d_A & \cos k_{zA}d_A \end{bmatrix}, \tag{5}$$

$$M_B = \begin{bmatrix} \cos k_{zB} d_B & \frac{\mathrm{i}}{\zeta_B} \sin k_{zB} d_B \\ \mathrm{i}\zeta_B \sin k_{zB} d_B & \cos k_{zB} d_B \end{bmatrix}, \tag{6}$$

$$M_g = \begin{bmatrix} 1 & 0 \\ \sigma_g & 1 \end{bmatrix}, \tag{7}$$

with $\zeta_A = \frac{-k_{zA}}{\omega}$, $\zeta_B = \frac{-k_{zA}}{\omega}$, $k_{zA} = k_0\sqrt{\varepsilon_A - \beta^2}$ and $k_{zB} = k_0\sqrt{\varepsilon_B - \beta^2}$. The eigenvector of M is then given by [45]:

$$\psi_{PC} = \begin{bmatrix} M_{1,2} \\ K_B d - M_{1,1} \end{bmatrix}, \tag{8}$$

where $M_{i,j}$ $(i, j = 1, 2)$ are elements of the transfer matrix M, $d = d_A + d_B$ and $K_B d$ is given as:

$$K_B d = \frac{M_{1,1} + M_{2,2}}{2} \pm \sqrt{\left(\frac{M_{1,1} + M_{2,2}}{2}\right)^2 - 1}\,. \tag{9}$$

To obtain the dispersion of the Tamm states, we must apply the electromagnetic boundary conditions at the interface of the nonlinear slab and the GBPC. To do this, we need the electromagnetic fields inside the nonlinear slab, which we can obtain them using the nonlinear transfer matrix method. Since the slab is nonlinear and the electromagnetic fields inside the slab depend on the amplitude of the electric field, we assume that the slab is composed of N sublayers. We choose the number of sublayers so that the spatial variations of the electric field within each sublayer to be negligible. Hence, the permittivity within the jth sublayer can be assumed to be constant: $\varepsilon_j = \varepsilon_S + \alpha|E(z = -(j-1)d_S/N)|^2$. Then, we use the transfer matrix method to obtain the electromagnetic fields inside the nonlinear slab at $z = -jd_S/N$ as: $\psi(z = -jd_S/N) = M_j \times \psi(z = -(j-1)d_S/N)$ where

$$M_j = \begin{bmatrix} \cos k_{zj} d_s/N & -\frac{\mathrm{i}}{\zeta_j} \sin k_{zj} d_s \Big/ N \\ -\mathrm{i}\zeta_j \sin k_{zj} d_s/N & \cos k_{zj} d_s/N \end{bmatrix}, \tag{10}$$

indicates transfer matrix of jth sub-layer, $\zeta_j = \frac{-k_{zj}}{\omega}$, $k_{zj} = k_0\sqrt{\varepsilon_j - \beta^2}$, $\psi(z = -jd_S/N)$ and $\psi(z = -(j-1)d_S/N)$ denote the electromagnetic fields in two adjacent sublayers. Finally, the electromagnetic fields at $z = 0$ are obtained in terms of the electromagnetic fields at $z = -d_S$ as follows [46]:

$$\psi(z = 0) = \left(\prod_{j=1}^{N} M_j\right) \times \psi(z = -d_S). \tag{11}$$

Using the boundary conditions at $z = -d_S$, the eigenvector $\psi(z = -d_S)$ is given as:

$$\psi(z = -d_S) = \begin{bmatrix} 1 \\ \zeta_u \end{bmatrix} E_0. \tag{12}$$

Here, $\zeta_u = \mathrm{i}q_u/\omega$ and $q_u = k_u/k_0$. To find the dispersion of the Tamm states, we satisfy the boundary conditions for the tangential components of the electric and magnetic fields at $z = 0$ using equations (8)–(12), to obtain

$$\begin{bmatrix} M_{1,2} \\ K_B d - M_{1,1} \end{bmatrix} = \left(\prod_{j=1}^{N} M_j\right) \times \begin{bmatrix} 1 \\ \zeta_u \end{bmatrix} E_0, \tag{13}$$

and numerically solve it.

3. Results and discussion

As a model system, the SiO_2 and polyethylene as dielectric materials of A and B were chosen, respectively. In our calculations, the thicknesses and the relative permittivities are according to [47, 48]. Therefore, the calculations were carried out using the values $\varepsilon_A = 4.84$, $\varepsilon_B = 2.29$, $\varepsilon_0 = 1$, $\varepsilon_S = 2.4025$(polydiacetylene: 9 − BCMU), $d_A = 10\,\mu$m , $d_B = 10\,\mu$m and $T = 300$ K. Although in theoretical calculations, we considered a semi-infinite GBPC, in practice, to avoid the manufacturing difficulty, it must have finite periods. Experimentally, the 1D GBPC may be fabricated through the thermal evaporation procedure [49]. Motivated with the experimental realization of a 1D structure composed of five periods of alternating graphene and Al_2O_3 layers by Chang *et al* [50], we consider a 1D GBPC of 5 periods and investigate its optical properties. It is quite straightforward to use the transition matrix method to obtain the reflection and transmission coefficients of the 1D GBPC as $R = \frac{\mathbb{M}_{11} - \mathbb{M}_{22} + \zeta_B\mathbb{M}_{12} - \mathbb{M}_{21}/\zeta_B}{\mathbb{M}_{11} + \mathbb{M}_{22} + \zeta_B\mathbb{M}_{12} + \mathbb{M}_{21}/\zeta_B}$ and $T = \frac{2}{\mathbb{M}_{11} + \mathbb{M}_{22} + \zeta_B\mathbb{M}_{12} + \mathbb{M}_{21}/\zeta_B}$, respectively [37]. Here, $\mathbb{M}_{i,j}$ $(i, j = 1, 2)$ are elements of the transfer matrix $\mathbb{M} = (M_A^{-1}M_G^{-1}M_B^{-1}M_G^{-1})^5$. Figure 2(a) shows the transmission of the 1D GBPC with the structure $(AGBG)^5$ on the plane of frequency and β as shown in figure 2(a). In the figure, the dark and bright regions show the forbidden and propagation bands of the considered structure, respectively. We consider the frequency interval 0–9 THz in which the real part of the graphene conductivity $\sigma_g(\omega)$ is negligible [51]. At this frequency interval, the structure shows two bandgaps. The first bandgap, which is attributed to the existence of the graphene monolayers in the structure, is a graphene induced photonic band gap (GIPBG) and the second one is the conventional Bragg gap [31]. To compare the quality of the GIPBG and the Bragg gap, we plotted the fineness $F = \frac{\pi\sqrt{R}}{1-R}$ of the structure as a function of β at two typical frequencies $f = 1$ THz and $f = 5.5$ THz in figure 2(b). The figure reveals that the fineness of the structure at the GIPBG is higher than its fineness at the Bragg gap and increases by increasing beta. Here, we assume the chemical potential of the graphene monolayers to be 0.2 eV. The chemical potential of graphene can be changed by applying an appropriate voltage or doping. Adjusting the chemical potential of graphene modifies the conductivity of graphene. By controlling the conductivity of graphene, one can control the characteristics (the bandwidth and the central frequency) of the bandgaps [51]. Due to the controllable bandgaps, studying the dispersion behavior of Tamm states in the GBPCs may be of great importance.

The dispersion properties of the Tamm states are summarized in the first two bandgaps of the GBPC on the plane of frequency versus β (see figure 3(a)). The figure shows the dispersion of the Tamm states for different width of the slab.

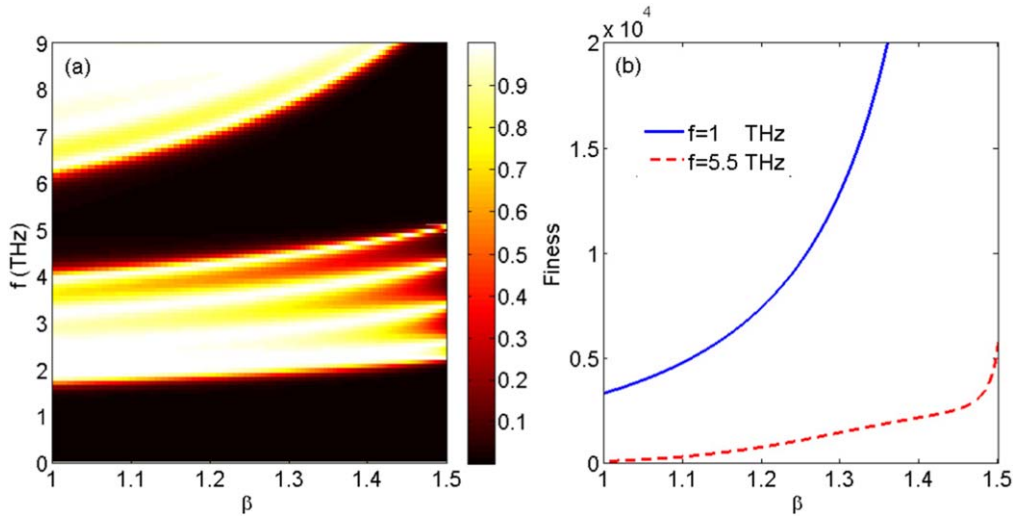

Figure 2. (a) The transmission of the 1D GBPC structure $(AGBG)^5$ on the plane of (f, β) and (b) the fineness of the structure as a function of β at two typical frequencies $f = 1$ THz (the solid line) and $f = 5.5$ THz (the dashed line), respectively. Here, the dark and bright regions show the forbidden and propagation bands of the considered structure, respectively. The other parameters are same as figure 1.

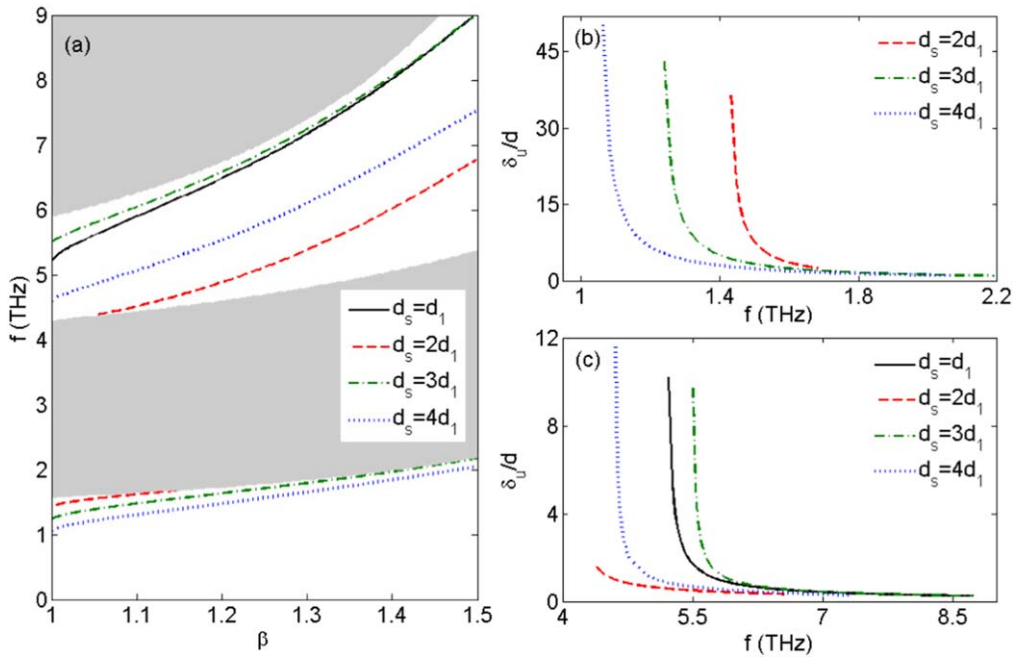

Figure 3. (a) The dispersion of the Tamm states versus β for different width of the nonlinear slab. The penetration depth of the Tamm states of (b) the GIPBG and (c) the Bragg gap in the uniform medium versus the frequency, respectively. The thicknesses of the nonlinear slab are assumed to be $d_S = d_A$ (the solid line), $d_S = 2\,d_A$ (the dashed lines), $d_S = 3\,d_A$ (the dashed–dotted lines) and $d_S = 4\,d_A$ (the dotted lines) with $\alpha|E_0|^2 = 0.1\,\varepsilon_S$ and $\mu_c = 0.2$ eV. Here, the dark and bright regions show the propagation and forbidden bands of the considered structure, respectively. The other parameters are same as figure 1.

We need an appropriate criterion for comparing surface waves in terms of their intensity. We consider this criterion as the intensity of surface waves at the interface between the uniform medium and the nonlinear slab, and we use the dimensionless intensity $\alpha|E_0|^2$ to show it. Here we assume that $\alpha|E_0|^2 = 0.1\,\varepsilon_S$. In the figure, the dark and bright regions show the propagation and forbidden bands of the considered structure, respectively.

Note that in the GIPBG there is no dispersion curve for $d_S = d_A$. This means that the dispersion equation has a solution only for the specific thicknesses of the nonlinear slab (here, $d_S = 2\,d_A, 3\,d_A, 4\,d_A$). Besides, the dispersion curves of the Tamm states move away from the edge of the GIPBG and experience a redshift as the nonlinear slab thickness increases (see figure 3(a)). However, the situation is quite different at the Bragg gap. Here, the dispersion equation has solutions for all considered slab thicknesses. The dispersion curves of the Tamm states in the Bragg gap also shift to lower frequencies as the thickness of the nonlinear layer increases. The shift of the modes ends by reaching the lower limit of the Bragg gap.

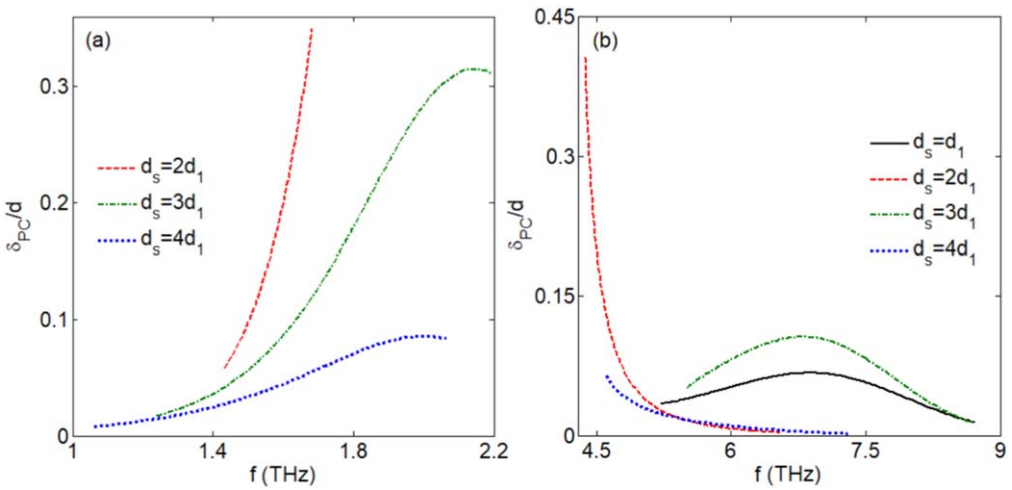

Figure 4. The penetration depth of the Tamm states of (a) the GIPBG and (b) the Bragg gap in the GBPC versus the frequency, respectively. Here, the thicknesses of the nonlinear slab are assumed to be $d_S = d_A$ (the solid line), $d_S = 2\,d_A$ (the dashed lines), $d_S = 3\,d_A$ (the dashed–dotted lines) and $d_S = 4\,d_A$ (the dotted lines) with $\alpha|E_0|^2 = 0.1\,\varepsilon_S$ and $\mu_c = 0.2$ eV. The other parameters are same as figure 1.

Then the Tamm states emerge from the upper edge of the bandgap and resume moving to the lower frequencies as the slab thickness increases.

To get a more profound insight into the Tamm states of both band gaps, we investigate their penetration depth in the left homogenous medium. The penetration depth of the Tamm states in the uniform medium (δ_u) is given as $\delta_u = 1/\mathrm{Re}(k_u)$. The figures 3(b) and (c) show the penetration depth of the Tamm states of the GIPBG and the Bragg gap in the uniform medium versus the frequency, respectively. We can see that for the specified thickness of the nonlinear layer, the modes of both bandgaps have high penetration depths at low frequencies (equivalently small β). However, the penetration depth of the Tamm states of the GIPBG is several times grater than that of the Bragg gap modes. Further, the penetration depth of the modes of both band gaps decreases and eventually becomes independent of the thickness of the nonlinear layer for the high-frequency Tamm states. Since the Tamm state of a given frequency with the highest β have the lowest penetration depth, the penetration depth of the surface modes can be adjusted by choosing the appropriate thickness for the nonlinear slab. The localized modes (the modes with the least penetration depth) of both bandgaps may have potential application in sensing devices, especially the biosensors [52]. Besides, the penetration depth of the Tamm states in the 1D GBPC (δ_{PC}) is given as $\delta_{\mathrm{PC}} = 1/\mathrm{Im}(K_{\mathrm{B}})$. In figure 4 the penetration depth of the Tamm states of (a) the GIPBG and (b) the Bragg gap are plotted as functions of the frequency. As the figure reveals, the penetration depth of the modes in the PC is much less than the depth of penetration into the uniform medium. Here, unlike the uniform medium, the Tamm state closer to the upper edge of the corresponding bandgap has the most depth of penetration into the GBPC.

Now, we want to study the effect of increasing the intensity on the dispersion curves of the Tamm states for a specified thickness of the nonlinear slab. The figure 5(a) shows the dispersion curves of the Tamm states for three different intensities $\alpha|E_0|^2 = 0.1\varepsilon_L$ (the solid lines), $0.3\varepsilon_L$ (the dashed lines), and $0.5\varepsilon_L$ (the dashed–dotted lines) at the interface between the nonlinear slab and the GBPC ($z = 0$) with $d_S = 4\,d_A$. As it is clear, increasing the intensity shifts the dispersion curves of the Tamm states of both bandgaps towards the lower frequencies. The penetration depth of the Tamm states of (b) the GIPBG and (c) the Bragg gap in the uniform medium are plotted versus the frequency for the intensities $\alpha|E_0|^2 = 0.1\varepsilon_L$ (the solid lines), $0.3\varepsilon_L$ (the dashed lines), and $0.5\varepsilon_L$ (the dashed–dotted lines) of the modes at $z = 0$ in figure 5. The figure shows that at a given frequency, in both band gaps, the penetration depth of the modes in the homogeneous medium decreases with increasing intensity. Consequently, one can control the frequency and localization length of the nonlinear Tamm states by adjusting the intensity of surface waves.

It is well known that the chemical potential and hence the conductivity of the graphene monolayer is modified by doping or applying a gate voltage. On the other hand, the dispersion equation (13) depends on the conductivity of the graphene sheets. So, it is interesting to investigate how the dispersion curves of the Tamm states affected by varying the conductivity of the graphene layers. To do this, we plotted the dispersion curves of the Tamm states as a function of the chemical potential of the graphene monolayers (μ_c) at $\beta = 1.1$ (the solid line), $\beta = 1.15$ (the dashed lines) and $\beta = 1.2$ (the dotted–dashed lines) in figure 6(a). Here, $\alpha|E_0|^2 = 0.1\varepsilon_L$ and $d_S = 4\,d_A$. It is seen that increasing the chemical potential increases the bandwidth of the GIPBG more effectively than the conventional Bragg gap. Additionally, the central frequency of the GIPBG undergoes a substantial blue shift than the Bragg gap by increasing chemical potential. Moreover, the frequency of the Tamm states of both bandgaps slightly shifts to higher frequencies by increasing the chemical potential. The penetration depth of the Tamm states of (b) the GIPBG and (c) the Bragg gap in the uniform medium are plotted versus the frequency at $\beta = 1.1$ (the solid line), $\beta = 1.15$ (the dashed lines) and $\beta = 1.2$ (the dotted–

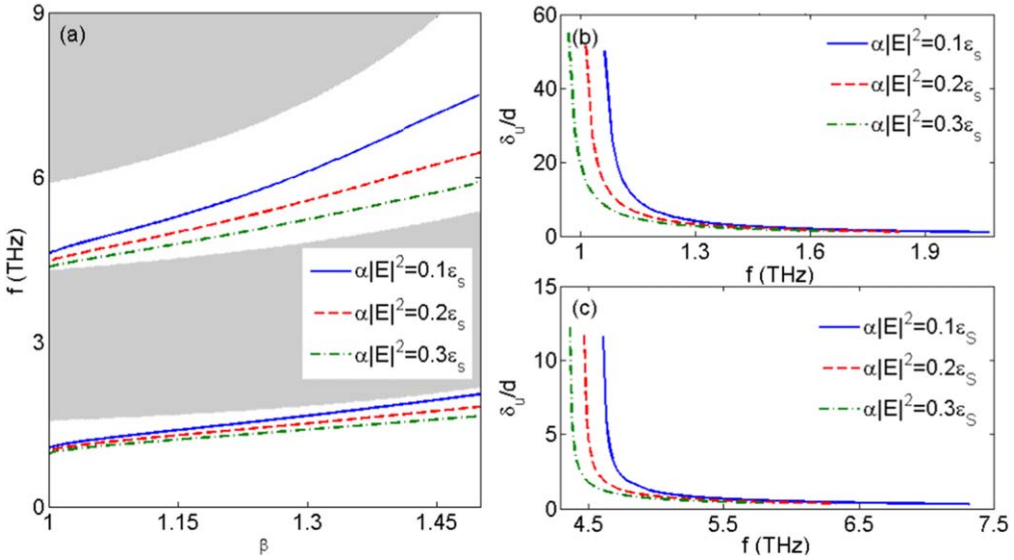

Figure 5. (a) The dispersion of the Tamm states versus β for different intensities of the Tamm states at the interface between the nonlinear slab and the GBPC. The penetration depth of the Tamm states of (b) the GIPBG and (c) the Bragg gap in the uniform medium versus the frequency, respectively. The intensities of the Tamm states at the interface between the nonlinear slab and the GBPC are assumed to be $\alpha|E_0|^2 = 0.1\,\varepsilon_S$ (the solid line), $\alpha|E_0|^2 = 0.2\,\varepsilon_S$ (the dashed lines) and $\alpha|E_0|^2 = 0.3\,\varepsilon_S$ (the dotted–dashed lines) with $d_S = 4\,d_A$ and $\mu_c = 0.2$ eV. Here, the dark and bright regions show the propagation and forbidden bands of the considered structure, respectively. The other parameters are same as figure 1.

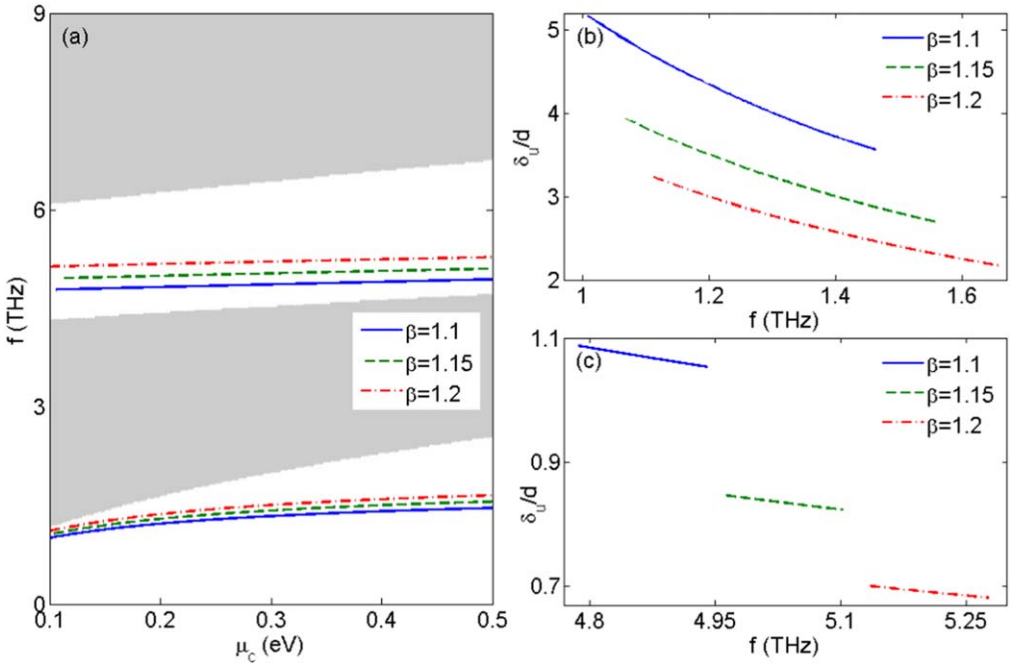

Figure 6. (a) The dispersion of the Tamm states versus chemical potential of graphene μ_c for different β with $\beta = 1.1$ (the solid line), $\beta = 1.15$ (the dashed lines) and $\beta = 1.2$ (the dotted–dashed lines). The penetration depth of the Tamm states of (b) the GIPBG and (c) the Bragg gap in the uniform medium versus the frequency, respectively. Here, the dark and bright regions show the propagation and forbidden bands of the considered structure respectively, $\alpha|E_0|^2 = 0.1\,\varepsilon_S$, $d_S = 4\,d_A$ and $\mu_c = 0.2$ eV. The other parameters are same as figure 1.

dashed lines) respectively, in figure 6. Here, the penetration depth of the Tamm states of both bandgaps decreases by increasing the chemical potential of graphene.

4. Conclusion

In summary, the dispersion properties of the TE-polarized Tamm states were investigated in the terahertz regime at the interface of a nonlinear Kerr-type dielectric slab and a 1D GBPC. The band structure of the PC under study contains one graphene induced bandgap and one Bragg gap in the desired

frequency range, which both of them support Tamm states of different characteristics. The dispersion of the Tamm states depends on the thickness of the nonlinear slab, the intensity of the surface modes, and the chemical potential of the graphene layers. That is, the surface modes are red-shifted with increasing the thickness of the nonlinear slab or the intensity, whereas they are blue-shifted with increasing the chemical potential. Since adjusting the thickness of the nonlinear slab means replacing it with a new one and changing the chemical potential of graphene is also not an easy task, it seems that the only effective way to adjust the dispersion of the Tamm states is to change the intensity of the modes. We have shown that the penetration depth of the graphene induced bandgap modes in the uniform environment is several times greater than that of the Bragg gap modes. Also, we observed that the penetration depth of the Tamm states decreases with increasing frequency and eventually becomes independent of the nonlinear slab thickness and intensity of the modes. At a given frequency, the Tamm state with the highest β has the least penetration depth. Therefore, we can alter the penetration depth of the surface modes by adjusting the thickness of the nonlinear slab, the intensity of the Tamm states, or the chemical potential of the graphene layers.

ORCID iDs

Samad Roshan Entezar https://orcid.org/0000-0003-1699-9114

References

[1] Li N, Tang T, Li J, Luo L, Sun P and Yao J 2018 Highly sensitive sensors of fluid detection based on magneto-optical optical Tamm state *Sensors Actuators* B **265** 644–51

[2] Gunasekaran C, Kumar B S, Ayyanar N, Raja G T and Mohan R 2019 Surface-plasmon-based photonic crystal fibers for high-bandwidth filter realization *J. Opt. Soc. Am.* B **36** 1574–80

[3] Mayevsky A D, Davis T J, Ballard P M, Henderson C A and Funston A M 2018 Mesoscale surface plasmons: modelling and imaging using near-field scanning optical microscopy *Opt. Express* **26** 23426–35

[4] Cai M, Wang S, Gao B, Wang Y, Han T and Liu H 2019 A new electro-optical switch modulator based on the surface plasmon polaritons of graphene in mid-infrared band *Sensors* **19** 89

[5] Wan Y, Zheng Z, Kong W, Zhao X, Liu Y, Bian Y and Liu J 2012 Nearly three orders of magnitude enhancement of Goos–Hanchen shift by exciting Bloch surface wave *Opt. Express* **20** 8998–9003

[6] Vukovic S M, Shadrivov I V and Kivshar Y S 2009 Surface Bloch waves in metamaterial and metal-dielectric superlattices *Appl. Phys. Lett.* **95** 041902

[7] Mills D L and Agranovich V M 1982 *Surface Polaritons: Electromagnetic Waves at Surfaces and Interfaces* (Amsterdam: North-Holland)

[8] McGilp J F, Weaire D and Patterson C 2012 *Epioptics: Linear and Nonlinear Optical Spectroscopy of Surfaces and Interfaces* (Brussels, Luxembourg: Springer Science & Business Media) 13:978-3-642-79822-1

[9] Yeh P, Yariv A and Cho A 1978 Optical surface waves in periodic layered media *Appl. Phys. Lett.* **32** 104–5

[10] Yeh P, Yariv A and Hong C S 1977 Electromagnetic propagation in periodic stratified media: I. General theory *J. Opt. Soc. Am.* **67** 423–38

[11] Eyni Z, Namdar A, Entezar S R and Tajalli H 2010 Dispersion properties of nonlinear surface waves in one-dimensional photonic crystals with a nonlinear self-defocusing cap layer of left-handed metamaterial *J. Opt. Soc. Am.* B **27** 2116–21

[12] Segovia-Chaves F and Vinck-Posada H 2019 Transmittance spectrum of a superconductor-semiconductor quasiperiodic one-dimensional photonic crystal *Physica* C **563** 10–5

[13] Sun Z, Jung Y S and Kim H K 2003 Role of surface plasmons in the optical interaction in metallic gratings with narrow slits *Appl. Phys. Lett.* **83** 3021–3

[14] Saleki Z, Entezar S R and Madani A 2017 Optical properties of a one-dimensional photonic crystal containing a graphene-based hyperbolic metamaterial defect layer *Appl. Opt.* **56** 317–23

[15] Hanson G W 2008 Quasi-transverse electromagnetic modes supported by a graphene parallelplate waveguide *J. Appl. Phys.* **104** 084314

[16] Geim A K 2009 Graphene: status and prospects *Science* **324** 1530–4

[17] Novoselov K S, Geim A K, Morozov S V, Jiang D, Zhang Y, Dubonos S V, Grigorieva I V and Firsov A A 2004 Electric field efect in atomically thin carbon films *Science* **306** 666–9

[18] Nair R R, Blake P, Grigorenko A N, Novoselov K S, Booth T J, Stauber T, Peres N M and Geim A K 2008 Fine structure constant defines visual transparency of graphene *Science* **320** 1308

[19] Bonaccorso F, Sun Z, Hasan T and Ferrari A 2010 Graphene photonics and optoelectronics *Nat. Photon.* **4** 611–22

[20] Low T and Avouris P 2014 Graphene plasmonics for terahertz to mid-infrared applications *ACS Nano* **8** 1086–101

[21] Chen C F *et al* 2011 Controlling inelastic light scattering quantum pathways in graphene *Nature* **471** 617–20

[22] Mikhailov S and Ziegler K 2007 New electromagnetic mode in graphene *Phys. Rev. Lett.* **99** 016803

[23] Hanson G W 2008 Dyadic Greens functions and guided surface waves for a surface conductivity model of graphene *J. Appl. Phys.* **103** 064302

[24] Ju L *et al* 2011 Graphene plasmonics for tunable terahertz metamaterials *Nat. Nanotechnol.* **6** 630–4

[25] Koppens F H, Chang D E and Garcia de Abajo F J 2011 Graphene plasmonics: a platform for strong light-matter interactions *Nano Lett.* **11** 3370–7

[26] Lin I T, Liu J M, Shi K Y, Tseng P S, Wu K H, Luo C W and Li L J 2012 Terahertz optical properties of multilayer graphene: Experimental observation of strong dependence on stacking arrangements and misorientation angles *Phys. Rev.* B **86** 235446

[27] Geim A K and Novoselov K S 2007 The rise of graphene *Nat. Mater.* **6** 183–91

[28] Chang Y C, Liu C H, Liu C H, Zhang S, Marder S R, Narimanov E E, Zhong Z and Norris T B 2016 Realization of mid-infrared graphene hyperbolic metamaterials *Nat. Commun.* **7** 3054–62

[29] Bludov Y V, Peres N M and Vasilevskiy M I 2012 Graphene-based polaritonic crystal *Phys. Rev.* B **85** 245409

[30] Bludov Y V, Ferreira A, Peres N and Vasilevskiy M 2013 A primer on surface plasmonpolaritons in graphene *Int. J. Mod. Phys.* B **27** 1341001

[31] Madani A and Entezar S R 2014 Surface polaritons of one-dimensional photonic crystals containing graphene monolayers *Superlattices Microstruct.* **75** 692–700

[32] Fan H M, Wang T B, Liu N H, Liu J T, Liao Q H and Yu T B 2014 Tunable plasmonic band gap and defect mode in one-

dimensional photonic crystal covered with graphene *J. Opt.* **16** 125005
[33] Chen Y, Dong J, Liu T, Zhu Q and Chen W 2016 Refractive index sensing performance analysis of photonic crystal containing graphene based on optical Tamm state *Mod. Phys. Lett.* B **30** 1650030
[34] Gorbach A 2013 Nonlinear graphene plasmonics: amplitude equation for surface plasmons *Phys. Rev.* A **87** 013830
[35] Huang Y and Hua Wu L 2014 Nonlinear TE-polarized surface plasmons at the interface between graphene and metamaterials *Advanced Materials Research* **933** 47–51
[36] Zheng Z, Jiang L, Guo J, Dai X and Xiang Y 2017 Tunable optical bistability in one-dimensional photonic crystal with a nonlinear defect coupled by graphene sheets *Adv. Condens. Matter Phys.* **2017** 6590424
[37] Ghasemi F, Roshan Entezar S and Razi S 2019 Terahertz tunable photonic crystal optical filter containing graphene and nonlinear electro-optic polymer *Laser Phys.* **29** 056201
[38] Moghaddam B T, Entezar S R, Safari E and Madani A 2017 Tunable surface waves in nonlinear graphene-based one-dimensional-photonic crystal *J. Nanophotonics* **11** 046010
[39] Shadrivov I V, Sukhorukov A A, Kivshar Y S, Zharov A A, Boardman A D and Egan P 2004 Nonlinear surface waves in left-handed materials *Phys. Rev.* E **69** 016617
[40] Entezar S R, Namdar A, Eyni Z and Tajalli H 2008 Nonlinear surface waves in onedimensional photonic crystals containing left-handed metamaterials *Phys. Rev.* A **78** 023816
[41] Pedersen T G, Flindt C, Pedersen J, Jauho A P, Mortensen N A and Pedersen K 2008 Optical properties of graphene antidot lattices *Phys. Rev.* B **77** 245431
[42] Stauber T, Peres N and Geim A 2008 Optical conductivity of graphene in the visible region of the spectrum *Phys. Rev.* B **78** 085432
[43] Falkovsky L and Pershoguba S 2007 Optical far-infrared properties of a graphene monolayer and multilayer *Phys. Rev.* B **76** 153410
[44] Yariv A and Yeh P 1984 *Optical Waves in Crystals* 10 (New York: Wiley)
[45] Yeh P 2005 *Optical Waves in Layered Media* 61 (New York: Wiley-Interscience)
[46] Vetrov S Y, Timofeev I V and Shabanov A V 2007 Influence of cubic nonlinearity on laser radiation transmission in a photonic crystal with spatially modified media properties *Phys. Status Solidi* **1** 92–4
[47] Hung H C, Wu C J and Chang S J 2011 Terahertz temperature-dependent defect mode in a semiconductor-dielectric photonic crystal *J. Appl. Phys.* **110** 093110
[48] Palik E D 1998 *Handbook of Optical Constants of Solids* 3 (New York: Academic)
[49] Xiang Y, Guo J, Dai X, Wen S and Tang D 2014 Engineered surface Bloch waves in graphene-based hyperbolic metamaterials *Opt. Express* **22** 3054–62
[50] Chang Y C, Liu C H, Liu C H, Zhang S, Marder S R, Narimanov E E, Zhong Z and Norris T B 2016 Realization of mid-infrared graphene hyperbolic metamaterials *Nat. Commun.* **7** 3054–62
[51] Madani A and Entezar S R 2013 Optical properties of one-dimensional photonic crystals containing graphene sheets *Physica* B **431** 1–5
[52] Baghbadorani H K, Barvestani J and Entezar S R 2017 Biosensors based on Bloch surface waves in one-dimensional photonic crystal with graphene nanolayers *Appl. Opt.* **56** 462–9